J Mater Sci: Mater Electron (2015) 26:3840–3852
DOI 10.1007/s10854-015-2910-x

Significant change in micro mechanical, structural and electrical properties of MgB_2 superconducting ceramics depending on argon ambient pressure and annealing duration

O. Ozturk[1,2] · E. Asikuzun[1] · S. Kaya[1,2]

Received: 18 December 2014 / Accepted: 3 March 2015 / Published online: 8 March 2015

Abstract In this study, the effects of different Ar pressure (vacuum, 0, 10 and 20 bar) and different annealing times (0.5 and 1 h) on microstructural, mechanical and superconducting properties of the bulk superconducting MgB_2 are investigated. The samples are produced using the solid state reaction method. X-ray diffraction and scanning electron microscopy measurements are performed for phase formation, crystal structure, lattice parameters, particle size analysis, grain orientations, grain connectivity, and surface morphology of MgB_2 samples. The superconducting properties are studied by dc resistivity measurements. In this study we have focused on microhardness measurements to investigate the mechanical properties. Vickers microhardness test is employed for determination of mechanical properties of the samples. The experimental microhardness results are analyzed by Meyer's law, proportional sample resistance model, elastic–plastic deformation model, Hays Kendall (*HK*) approach, and indentation induced cracking (*IIC*) model. *HK* approach is identified as the most appropriate model for MgB_2 superconducting samples exhibiting the indentation size effect behavior; for the other samples that have reverse indentation size effect behavior *IIC* model is appointed as the most appropriate model.

✉ O. Ozturk
oozturk@kastamonu.edu.tr

[1] Department of Physics, Faculty of Arts and Science, Kastamonu University, 37100 Kastamonu, Turkey

[2] Research and Application Center, Kastamonu University, 37100 Kastamonu, Turkey

1 Introduction

The response of a material against the applied mechanical load is related to the mechanical properties. Basically, the mechanical properties arise from the inter-atomic bond properties of materials. The mechanical properties are closely related with structural, physical and chemical properties. In recent years, researchers have focused on studies towards improving and regulation of mechanical properties along with the developments in material science. While the structural and physical properties of materials can be arranged by variety of production processes, the chemical properties of a material can be arranged by different element and compound doping. The main mechanical properties are tensile/compression, impact, fracture, fatigue, creep and hardness. Among these properties, hardness is one of the most important parameters used to determine the mechanical properties of a solid in microscopic scale.

In this study, we have focused on the mechanical properties of superconducting MgB_2 in detail. The Vickers hardness test is used as the testing method. There are many studies related with mechanical characterization of superconducting MgB_2 in literature [1–3].

When we look at the Vickers hardness equation (Eq. 3), it is clearly seen that hardness varies the applied load in the solid. The variation of hardness with applied load varies according to the experimental conditions and the type of material. In literature, four types of variation of hardness with load are demonstrated. These four types of behavior are; decreasing, increasing, constant, and wavy behavior of hardness against the applied load.

The reduction of hardness with the increasing applied load is the most common result. After a certain value of the load, the variation in hardness is very small and the

hardness is independent of the load. This behavior is named as indentation size effect (*ISE*). There are many studies in the literature about *ISE*, the most commonly observed behavior [4–6].

The increasing of hardness with applied load is called the reverse indentation size effect (*RISE*), and as in the *ISE* case the variation of hardness with applied load becomes very small after a certain value of applied load. *RISE* behavior has not yet been fully explained until now and it is thought that it can be caused due to defects of the indenter, or cracks and fractures that occur during the indentation process. Although it is not as often as *ISE* behavior, there are available studies related with *RISE* behavior in the literature [1–3].

In some materials, hardness reaches to maximum and minimum points with the applied load. Although this type of behavior is rare, it has been observed in some organic crystals [7] and some polymeric materials [8].

The absence of a change in hardness with the applied load is the behavior of an ideal material and it has been observed in only a few materials [9, 10].

2 Preparation of samples

In this study, MgB_2 powder (Alfa Aesar, −325 mesh, <44 micron) is used. Tablets with 13 mm diameter and 1.0–1.5 mm thickness are prepared by pressing 6 g of powder using pressure of 7 tons. Bulk samples obtained by pressing are wrapped in the thallium (Ta) foil tightly to prevent oxidation. Samples wrapped in Ta foil are placed directly into a steel tube. The air in the steel tube is evacuated using a vacuum apparatus and then the furnace is heated to 850 °C from room temperature with 5 °C/min heating rate. Two sets of samples are produced, one with 0.5 h of annealing and the other for 1 h of annealing. The annealing procedure is repeated with unpressurized Ar atmosphere, with 10 and 20 bar Ar gas pressures. The produced samples are denoted as *MgB-05-V*, *MgB-05-0B*, *MgB-05-10B*, *MgB-05-20B* and *MgB-1-V*, *MgB-1-0B*, *MgB-1-10B*, *MgB-1-20B*. And finally, XRD, SEM, Vickers microhardness and dc resistivity (ρ-T) measurements are performed for structural, mechanical and electrical analysis of prepared MgB_2 samples.

3 Results and discussions

3.1 XRD analyses

X-ray diffraction measurements are carried out using a Bruker D8 Advance model XRD with CuKα target giving a monochromatic beam with wavelength 1.54 Å in the range $2\theta = 3°–90°$ at a scan speed of 0.6°/min and step increment of 0.02° at room temperature.

The XRD graphs of the MgB_2 samples are given in Fig. 1. For both series of samples, the peak intensities of the vacuum-produced samples are higher and the peaks are narrower than those of the samples produced under ambient pressure. Increasing Ar pressure causes peak intensities to decrease and the peaks to widen. Samples have better crystal structure under vacuum. The decrease in peak intensities may be due to the decrease in grain sizes as an effect of pressure. The results are tabulated in Table 1. Table 1 shows that in transition from vacuum to Ar ambient and by increasing Ar pressure, both *a* and *c* lattice parameters decrease. In previous studies, the applied pressure is confirmed to decrease the lattice parameters by shortening the bond lengths [11–13].

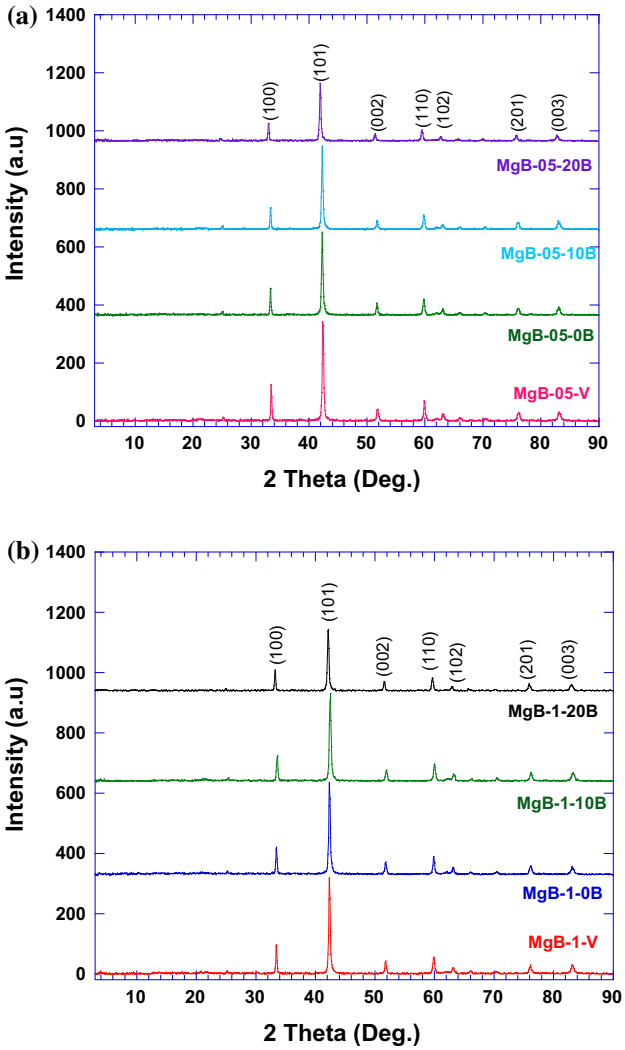

Fig. 1 XRD patterns of **a** 0.5 h annealed samples, **b** 1 h annealed samples

Moreover, the samples annealed for 1 h have longer *a* and *c* parameters when compared to the ones annealed for 0.5 h. This can be explained by the increased thermal expansion due to increased heat treatment time. Like other properties of MgB_2, anisotropy is seen in the change of lattice parameters. The change in *c* parameter is higher than the one in *a* parameter when the annealing time is increased which is consistent with previous studies [11].

Table 1 Lattice parameters and grain sizes of the samples

Samples	*a* (Å)	*c* (Å)	Grain size (nm)
MgB-05-V	3.098	3.527	36.86
MgB-05-0B	3.096	3.511	35.76
MgB-05-10B	3.096	3.509	34.27
MgB-05-20B	3.092	3.506	31.57
MgB-1-V	3.099	3.537	38.94
MgB-1-0B	3.098	3.531	36.05
MgB-1-10B	3.097	3.520	35.15
MgB-1-20B	3.093	3.508	32.14

3.2 SEM analysis

The grain size, grain connectivity and surface morphology of the samples are determined using a Jeol scanning electron microscope (SEM) JEOL 6390-LV, operated at 20 kV, with a resolution power of 3 nm.

SEM photographs of all samples are shown in Fig. 2. It is determined that samples show a granular structure that is characteristic morphology of MgB_2 samples. In addition there is no specific orientation of MgB_2 particles. When 0.5 and 1 h annealed samples are compared, the samples annealed for 0.5 h are more intensive and have less porosity than 1 h annealed samples. As it is known particle size of material increases with increasing the heat treatment time and heat treatment temperature [14]. Also, particle size decreases with increasing the pressure applied for each series. It can be said that gaps between particles decrease with decreasing the particle size (especially for *MgB-05-20B* and *MgB-1-20B*). The reduction of particle size directly affects the mechanical properties of samples due to the decrease in porosity. Therefore, we focused on characterization of mechanical properties of MgB_2 superconductor samples in this study.

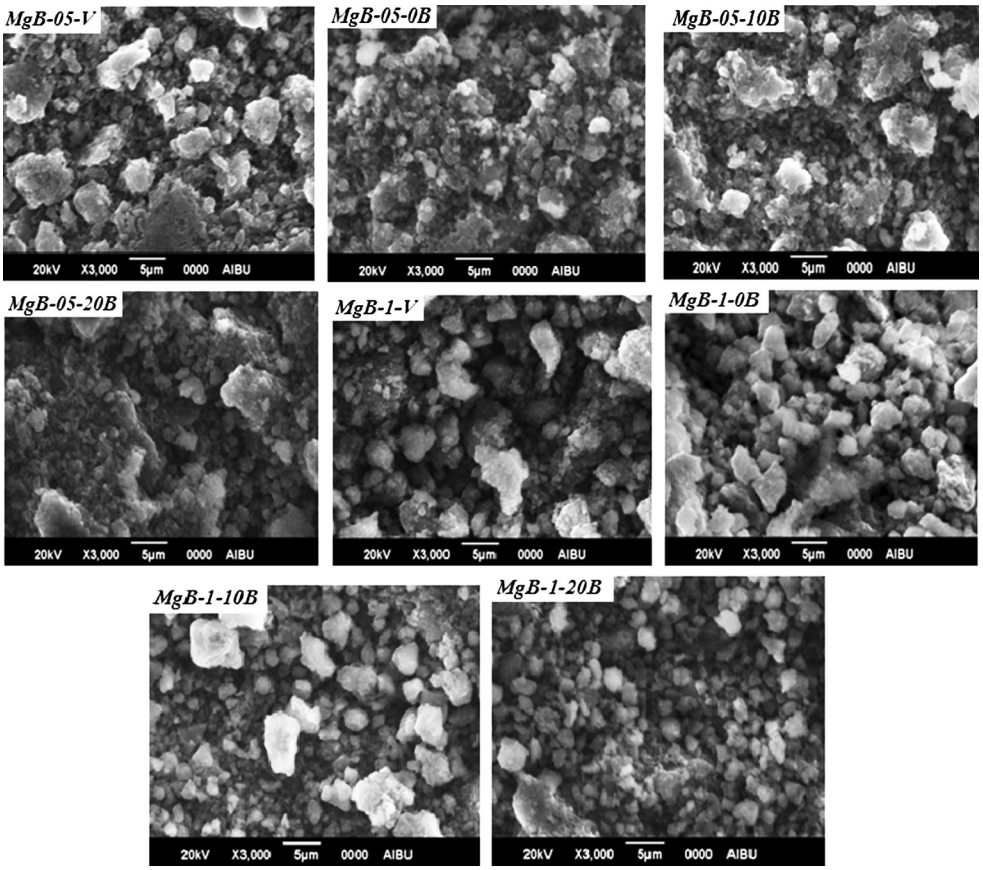

Fig. 2 SEM micrographs of the samples

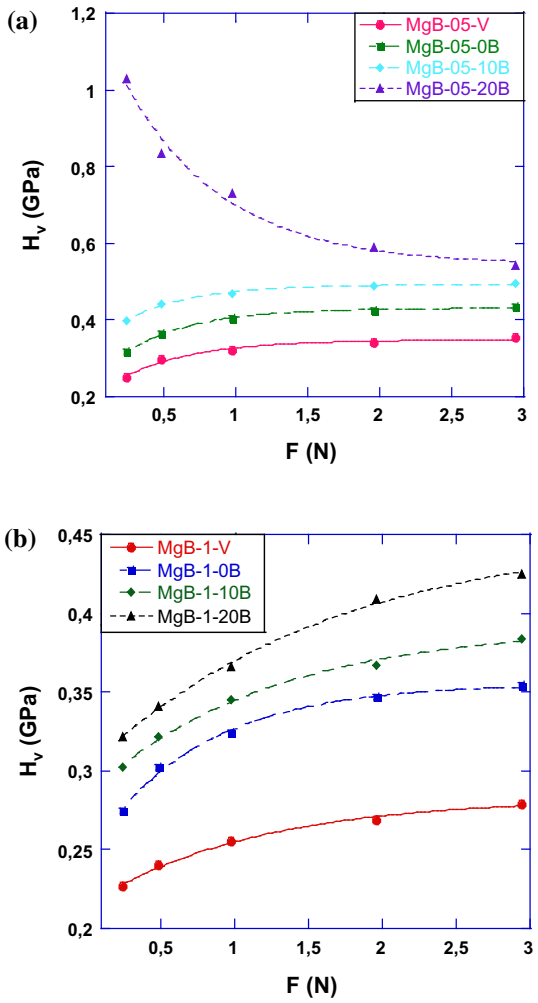

Fig. 3 The variations of microhardness values (H_V) with applied load **a** 0.5 h annealed samples, **b** 1 h annealed samples

3.3 Description of important mechanical parameters such as Vickers microhardness, elasticity modulus, yield strength, fracture toughness, brittleness, ductility

Vickers microhardness test is used for the determination of hardness values of MgB_2 samples produced in this study. Microhardness measurements of the samples are performed in air by using a digital microhardness tester (Shimadzu) at room temperature. The applied load is varied within the range 0.245–2.940 N for a peak-load time of 10 s and the diagonals of indentation are measured with an accuracy of ±0.1 μm. The values of Vickers microhardness are determined with an average of 20 readings at different locations of sample surfaces.

Vickers hardness test was developed to measure the hardness of materials as an alternative to Brinell method by Robert L. Smith and George E. Sandland in 1921. Vickers test is easier than the other tests because the required calculations are independent of the size of indenter and the indenter is used for all materials regardless of whatever the hardness value is.

The basic principle, as with all the general principles of hardness, shows the response of a material to resist to plastic deformation formed with a load applied from a source standard in the material. Vickers test can be used for all materials and has one of the widest scales among hardness tests. Hardness is determined by the force applied using indenter on the surface area. In our study, hardness unit is taken as GPa.

H_v hardness is determined by F/A ratio. F is applied load on the surface of material. A is surface area in terms of micrometers square. A can be calculated by the following formula:

$$A = \frac{d^2}{2\sin(136^\circ/2)} \tag{1}$$

$$A \approx \frac{d^2}{1854.4} \tag{2}$$

$$H_v = F/A \approx \frac{1854.4F}{d^2}\ \text{GPa} \tag{3}$$

Figure 3 shows changes of the microhardness values as a function of applied load. The hardness values calculated using Eq. 3 are given in Table 2. We can say that the microhardness of MgB_2 samples produced at different heat treatment times and different pressures depends on the applied load. Microhardness of all samples excluding the *MgB-05-20B* increases with applied load. This behavior is called reverse indentation size effect (*RISE*) behavior in the literature. The microhardness of *MgB-05-20B* sample decreases with increasing the applied load and this sample exhibits the indentation size effect (*ISE*) behavior. In addition, it can be clearly seen from the table, the samples produced in 0.5 h are harder than the samples produced in 1 h.

Parameters such as modulus of elasticity (E), brittleness (B_i), fracture toughness (K_{IC}), yield strength (Y) and ductility (D) that are as important as hardness for mechanical characterizations of materials are also calculated and the results are given in Table 2.

The modulus of elasticity (E) also referred to as Young's modulus is a measure of elastic deformation of the material under force. It is calculated as described below. With increasing E, the material becomes more rigid and shows less stress and deformation. When it decreases, the material behaves more flexible/elastic.

$$E = 81.9635\,H_V \tag{4}$$

Brittleness is the tendency against fracture of a material which is exposed to very little fracture or shows no predetermined deformation. It expresses the absence of plastic

Table 2 The load dependent H_v, E, Y, K_{IC}, B_i and D values of the samples

Samples	Load (N)	H_v (GPa)	E (GPa)	Y (GPa)	K_{IC} (Pa/m$^{1/2}$)	$Bi \times 10^3$ (m$^{1/2}$)	$D \times 10^{-4}$ (1/m$^{1/2}$)
MgB-05-V	0.245	0.252	20.654	0.084	388.296	648.99	15.409
	0.490	0.279	22.867	0.093	408.575	682.86	14.644
	0.980	0.322	26.392	0.107	438.932	733.60	13.631
	1.960	0.341	27.949	0.113	451.694	754.94	13.246
	2.940	0.353	28.933	0.117	459.576	768.10	13.019
MgB-05-0B	0.245	0.316	25.900	0.105	423.964	745.35	13.417
	0.490	0.366	29.998	0.122	456.213	802.26	12.465
	0.980	0.404	33.113	0.134	479.378	842.76	11.866
	1.960	0.425	34.834	0.141	491.678	864.39	11.569
	2.940	0.434	35.572	0.144	496.859	873.49	11.448
MgB-05-10B	0.245	0.398	32.621	0.132	410.273	970.09	10.308
	0.490	0.443	36.309	0.147	432.844	1023.5	9.7704
	0.980	0.469	38.440	0.156	445.365	1053.1	9.4958
	1.960	0.488	40.080	0.162	454.766	1073.1	9.3188
	2.940	0.499	40.890	0.166	459.339	1086.3	9.2056
MgB-05-20B	0.245	1.090	84.340	0.343	1130.00	910.62	10.982
	0.490	0.833	68.275	0.277	1016.70	819.32	12.205
	0.980	0.729	59.751	0.243	951.120	766.46	13.047
	1.960	0.588	48.194	0.196	854.199	688.36	14.527
	2.940	0.543	44.506	0.181	820.865	661.50	15.117
MgB-1-V	0.245	0.227	18.605	0.075	274.160	827.98	12.078
	0.490	0.240	19.671	0.080	281.905	851.35	11.746
	0.980	0.255	20.900	0.085	290.578	877.56	11.395
	1.960	0.269	22.048	0.089	298.452	901.32	11.095
	2.940	0.279	22.860	0.093	303.898	918.07	10.892
MgB-1-0B	0.245	0.275	22.539	0.091	346.926	792.68	12.615
	0.490	0.302	24.752	0.100	363.559	830.68	12.038
	0.980	0.324	26.556	0.108	376.575	860.39	11.623
	1.960	0.347	28.441	0.115	389.711	890.40	11.231
	2.940	0.354	29.015	0.118	393.624	899.34	11.119
MgB-1-10B	0.245	0.302	24.752	0.100	368.966	818.50	12.217
	0.490	0.322	26.392	0.107	380.993	845.16	11.832
	0.980	0.345	28.277	0.115	394.364	874.83	11.431
	1.960	0.367	30.080	0.122	406.743	902.29	11.083
	2.940	0.384	31.473	0.128	416.054	922.96	10.835
MgB-1-20B	0.245	0.322	26.392	0.107	440.732	730.60	13.687
	0.490	0.341	27.949	0.113	453.546	751.85	13.301
	0.980	0.366	29.998	0.122	469.877	778.93	12.838
	1.960	0.409	33.523	0.136	496.718	823.40	12.145
	2.940	0.425	34.834	0.141	506.338	839.36	11.914

deformation ability. Brittleness (B_i), is the opposite of ductility (D). Ductility is the ability of a material to permanent deformation.

$$B_i = H_v/K_{IC} \quad (5)$$

$$D = 1/B_i \quad (6)$$

The toughness of a material is the maximum amount of energy that is absorbed before fracture. And it is also described as the ability of the material to deform plastically. Toughness in brittle materials may be small because of elastic and plastic deformation allowing the majority of the energy to be absorbed by the material. In

Table 3 Regression analysis of experimental data according to Meyer's law

Samples	Slope n_k	$\ln_{Ak}$ (GPa)
MgB-05-V	2.321	−10.091
MgB-05-0B	2.283	−9.664
MgB-05-10B	2.190	−9.087
MgB-05-20B	1.591	−6.259
MgB-1-V	2.180	−9.694
MgB-1-0B	2.227	−9.643
MgB-1-10B	2.212	−9.499
MgB-1-20B	2.261	−9.620

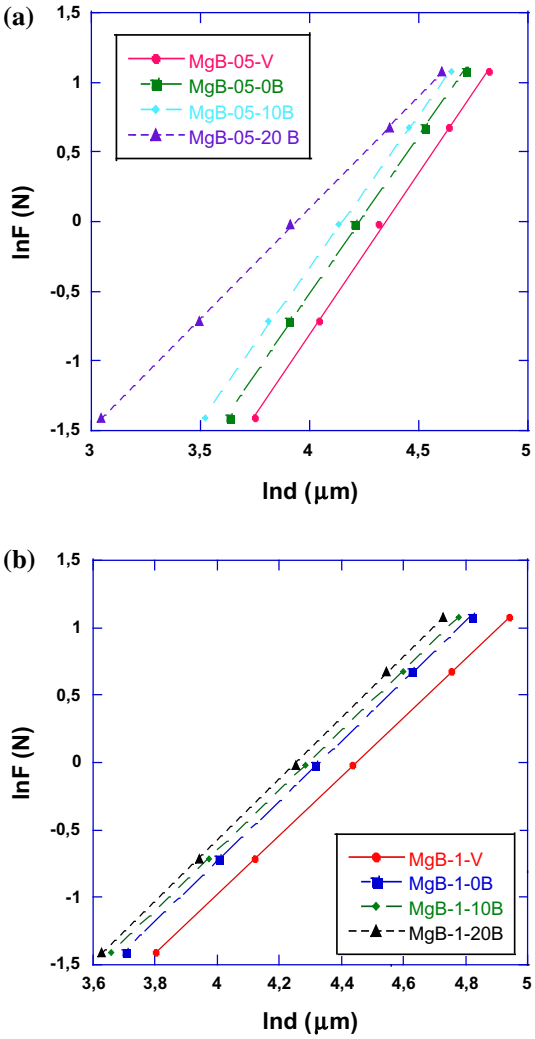

Fig. 4 Variation of ln$F$ with ln$d$ for **a** 0.5 h annealed samples, **b** 1 h annealed samples

materials science, fracture toughness is a property that defines the ability of the material which containing the cracks formed by breaking and is one of the most important features of any material in many design applications. Linear elastic fracture toughness of a material is determined by the formation of a crack emerging by stress intensity factor (K).

$$K_{IC} = \sqrt{2E\gamma} \tag{7}$$

Stress (yield strength) expresses the transition point from elastic deformation to plastic deformation.

$$Y \approx H_V/3 \tag{8}$$

As it can be seen from the table, elastic modulus (E), yield stress (Y), fracture toughness (K_{IC}) and brittleness (B_i) values of the materials produced in Ar atmosphere are higher than those of the materials produced in vacuum ambient in 0.5-h-series and when the pressure reaches to 10 and 20 bar, respectively, E, Y, K_{IC}, and B_i values increase. The brittleness of the material decreases with increasing K_{IC}. The data obtained from our samples verified this result clearly. Moreover, E, Y, K_{IC}, and B_i values in *MgB-05-V*, *MgB-05-0B*, *MgB-05-10B* samples increased with increasing applied load. However, these values decreased with the increase of the applied load in *MgB-05-20B* sample. This result is related to *ISE* behavior.

One can see that E, Y, K_{IC}, and B_i values of the samples produced in 1 h are lower than the materials produced in 0.5 h. Herein, E, Y, K_{IC} and B_i values of the samples produced in vacuum ambient is less than the samples produced in Ar atmosphere without pressure. With the applied pressure reaching to 10 and 20 bar, E values increased significantly. Besides, for all samples produced in 1 h, E, Y, and K_{IC} values increased.

In the literature, various theoretical models have been developed to analyze the *ISE* and *RISE* behavior of materials. These are; Meyer law, proportional sample resistance (*PSR*) model, Hays–Kendall (*HK*) model, elastic/plastic deformation model, and indentation induced cracks (*IIC*) model [15–20]. All the theoretical models have been applied to our samples in order to investigate the behavior of the hardness of samples with load and all the results are listed below.

3.4 Application of microhardness models

3.4.1 Meyer law

Meyer's law given by Eq. 9 is the simple experimental expression that is developed to investigate the *ISE* behavior of a sample [21].

$$F = Ad^n \tag{9}$$

The calculated values of Meyer index (n) of the samples are all higher than 2 except for the *MgB-05-20B* sample (Table 3) which confirm that *RISE* behavior is observed in

Table 4 Regression analysis of experimental data according to *PSR* model

Samples	$a_1 \times 10^{-3}$ (N)	$a_2 \times 10^{-5}$ (N/μm)	H_{PSR} (GPa)	H_V (GPa)
MgB-05-V	−3.65	21.91	0.406	0.341–0.353
MgB-05-0B	−3.47	26.54	0.492	0.425–0.434
MgB-05-10B	−2.58	29.34	0.544	0.488–0.499
MgB-05-20B	7.57	22.04	0.408	0.543–0.588
MgB-1-V	−2.02	16.32	0.302	0.269–0.279
MgB-1-0B	−2.67	21.17	0.392	0.347–0.354
MgB-1-10B	−2.75	22.71	0.425	0.367–0.384
MgB-1-20B	−3.68	25.86	0.479	0.409–0.425

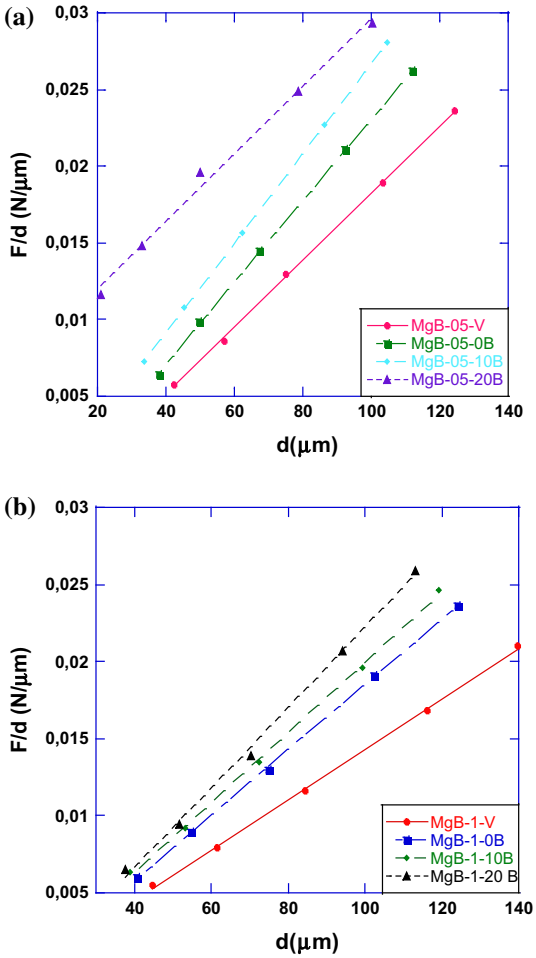

Fig. 5 Plots of *F/d* versus *d* for **a** 0.5 h annealed samples, **b** 1 h annealed samples

these samples (Fig. 4). Additionally, in *MgB-05-20B* sample, $n < 2$ confirms that *ISE* behavior is observed for this sample. In the literature, if the *"n"* value is between 1 and 1.6, the sample is defined as ''hard'', and if this value is higher than 1.6, the sample is ''soft'' [22]. $n > 2$ values given in Table 3 show that the samples (except *MgB-05-20B*) are soft and *MgB-05-20B* is a hard material.

3.4.2 PSR model

In this model, the sample resistance is not constant and it increases with the depth of the indentation (Eq. 10).

$$F = a_1 d + a_2 d^2 \tag{10}$$

As seen from the Table 4, for all the samples (except *MgB-05-20B*) a_1 is negative (Fig. 5). This verifies that only plastic deformation is observed in the materials which show *RISE* behavior. For *MgB-05-20B* sample, a_1 value is positive which confirms *ISE* behavior, and elastic deformation as well as plastic deformation is observed in the sample. In addition, using load-independent H_{PSR} value, the calculated values of load-independent elastic modulus (E_0), stress (Y_0), fracture toughness (K_{IC}), brittleness (B_i) and ductility (D) values are given in Table 5.

Quinn and Quinn (1997) observed that hardness values remain unchanged in the transition region which is named as the plateau region [23]. The hardness values corresponding to this region are referred to as the true hardness values. From the analysis of the hardness values of the samples, it can be seen that the plateau region is reached at 1960 N for the samples.

When the obtained load independent values (Table 5) and H_{PSR} (Table 4) hardness values are compared to the values corresponding to the plateau region, it is seen that these values are quite far from the plateau region. For this reason, *PSR* model is inadequate to determine the real hardness values of the samples.

3.4.3 EPD model

In many indentation tests, the size of the indentation is measured after the indenter has been removed from the sample surface. Elastic recovery occurs around the indentation trace after removing indenter. So that, it is deemed appropriate to add a new term to the measured indentation size in order to calculate the load independent hardness value considering that indentation size shrinks to a certain degree [24]. Considering this effect, *EPD*

Table 5 The load independent H_0, E_0, Y_0, K_{IC}, B_i and D values for the samples

Samples	H_0 (GPa)	E_0 (GPa)	Y_0 (GPa)	K_{IC} (Pa/m$^{1/2}$)	$Bi \times 10^3$ (m$^{1/2}$)	$D \times 10^{-4}$ (1/m$^{1/2}$)	H_v (GPa)
MgB-05-V	0.406	32.27	0.135	485.409	836.41	11.956	0.341–0.353
MgB-05-0B	0.491	40.24	0.163	528.482	929.08	10.763	0.425–0.434
MgB-05-10B	0.544	44.58	0.181	479.660	1134.1	8.8173	0.488–0.499
MgB-05-20B	0.371	30.40	0.123	678.510	546.79	18.289	0.543–0.588
MgB-1-V	0.302	24.75	0.100	316.224	955.02	10.471	0.269–0.279
MgB-1-0B	0.392	32.12	0.130	414.208	946.38	10.567	0.347–0.354
MgB-1-10B	0.425	34.83	0.141	437.706	970.97	10.299	0.367–0.384
MgB-1-20B	0.479	39.26	0.159	537.544	891.09	11.222	0.409–0.425

Table 6 Regression analysis of experimental data according to *EPD* model

Samples	$A_2^{1/2}$	d_e (μm)	H_{EPD} (GPa)	H_v (GPa)
MgB-05-V	0.014	−0.144	0.411	0.341–0.353
MgB-05-0B	0.016	−0.120	0.498	0.425–0.434
MgB-05-10B	0.017	−0.082	0.542	0.488–0.499
MgB-05-20B	0.015	0.193	0.434	0.543–0.588
MgB-1-V	0.012	−0.087	0.303	0.269–0.279
MgB-1-0B	0.016	−0.120	0.498	0.347–0.354
MgB-1-10B	0.015	−0.103	0.422	0.367–0.384
MgB-1-20B	0.016	−0.131	0.486	0.409–0.425

model's hardness value is found to follow the relationship:

$$F^{1/2} = A_1^{1/2} d_p + A_2^{1/2} d_e \quad (11)$$

There is no consistency between the H_{EPD} values and the corresponding H_v values of the plateau region (Table 6). It is also seen that d_e is negative for all the samples (except for *MgB-05-20B*) (Fig. 6). In other words, no elastic deformation is observed for applied loads. The *ISE* behavior observed in *MgB-05-20B* sample is due to both the elastic deformation as well as plastic deformation. Therefore, it can be said that *EPD* model is insufficient to explain the mechanical behavior of the samples.

3.4.4 HK approach

Hays and Kendall have suggested that there should be the minimum load value (W_{HK}) to create a permanent deformation in the sample. If the applied load does not exceed this resistance, permanent deformation does not occur and only elastic deformation takes place. There is only the elastic deformation under the limit value, above which, both plastic and elastic deformation may be formed [25].

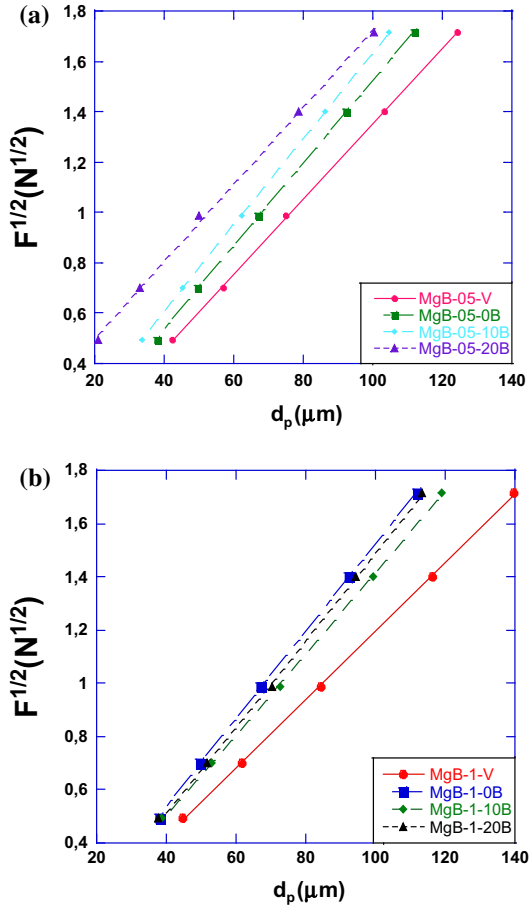

Fig. 6 Plots of $F^{1/2}$ versus d_p for **a** 0.5 h annealed samples, **b** 1 h annealed samples

This situation is observed by the sudden entry of the indenter into the sample above a critical load value. Also, before reaching a critical load value, it has been observed that the size of the indenter remains unchanged despite the increase in the test load. It is proposed that the experimentally measured dimension of the trace is

proportional to an effective $F_{eff} = F - W_{HK}$ instead of the applied load (F) through the relation as [26]:

$$F - W_{HK} = A_{1HK} d^2 \tag{12}$$

where W_{HK} is the minimum applied load to create indentation, and A_{1HK} is the load-independent hardness constant. The relation is depicted in Fig. 7. The calculated parameters are tabulated in Table 7. The W_{HK} value is positive for the *MgB-05-20B* sample, and it is negative for all other samples, which confirm that *MgB-05-20B* sample obeys *ISE* behavior whereas all other samples obey *RISE*. The positive value of W_{HK} (*MgB-05-20B*) shows that the

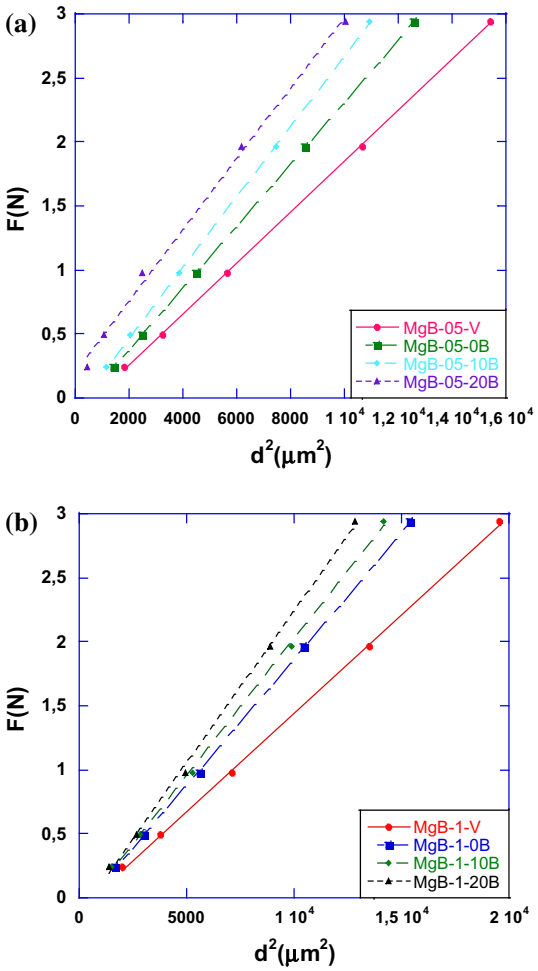

Fig. 7 Plots of F versus d_p^2 for **a** 0.5 h annealed samples, **b** 1 h annealed samples

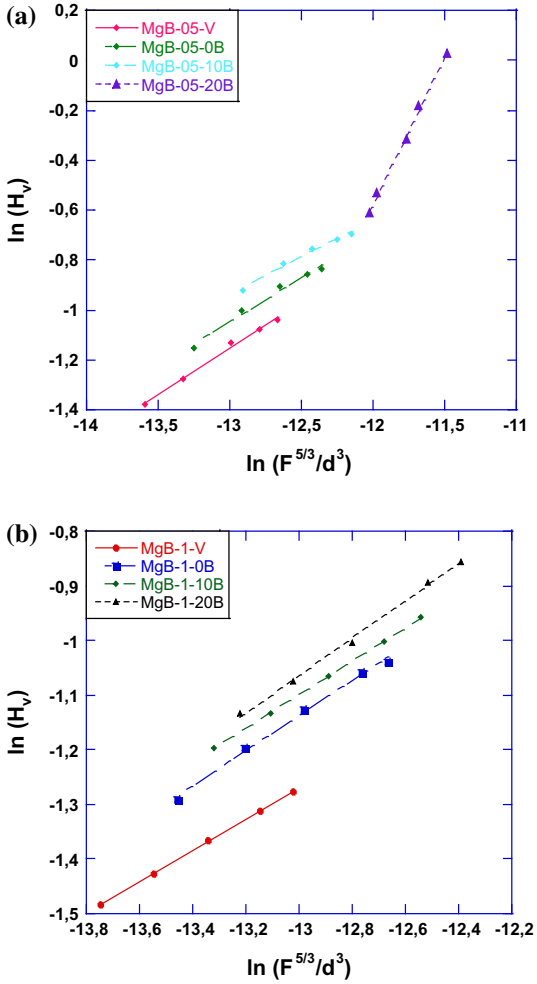

Fig. 8 Plots of $\ln(H_V)$ versus $\ln(F^{5/3}/d)^3$ according to *IIC* model for **a** 0.5 h annealed samples, **b** 1 h annealed samples

Table 7 Regression analysis of experimental data according to *HK* model

Samples	$A_{1HK} \times 10^{-5}$	W_{HK} (N)	n_{HK}	H_{HK} (GPa)	H_v (GPa)
MgB-05-V	19.83	−0.137	1.96	0.367	0.341–0.353
MgB-05-0B	24.24	−0.108	1.99	0.449	0.425–0.434
MgB-05-10B	27.52	−0.077	1.98	0.510	0.488–0.499
MgB-05-20B	27.74	0.1995	2.52	0.514	0.543–0.588
MgB-1-V	15.38	−0.910	1.13	0.285	0.269–0.279
MgB-1-0B	19.68	−0.099	1.96	0.364	0.347–0.354
MgB-1-10B	21.24	−0.108	1.92	0.393	0.367–0.384
MgB-1-20B	23.74	−0.140	2.94	0.440	0.409–0.425

Table 8 Regression analysis of experimental data according to *IIC* model

Samples	m	$K \times 10$ ($N^{(3-5\ m)/3}/\mu m^{(2-3\ m)}$)	H_{IIC} (GPa)	H_v (GPa)
MgB-05-V	0.373	3.69	0.307	0.341–0.353
MgB-05-0B	0.358	3.61	0.388	0.425–0.434
MgB-05-10B	0.297	2.92	0.457	0.488–0.499
MgB-05-20B	1.167	13.43	0.807	0.543–0.588
MgB-1-V	0.284	2.430	0.255	0.269–0.279
MgB-1-0B	0.320	3.031	0.322	0.347–0.354
MgB-1-10B	0.309	2.918	0.340	0.367–0.384
MgB-1-20B	0.341	3.372	0.372	0.409–0.425

Table 9 The results of load dependent Vickers microhardness at the plateau region and load independent hardness values calculated using *PSR*, *EPD*, *HK* and *IIC* models

Samples	H_{PSR} (GPa)	H_{EPD} (GPa)	H_{HK} (GPa)	H_{IIC} (GPa)	H_v (GPa)
MgB-05-V	0.406	0.411	0.367	0.307	0.341–0.353
MgB-05-0B	0.492	0.498	0.449	0.388	0.425–0.434
MgB-05-10B	0.544	0.542	0.510	0.457	0.488–0.499
MgB-05-20B	0.408	0.434	0.514	0.807	0.543–0.588
MgB-1-V	0.302	0.303	0.285	0.255	0.269–0.279
MgB-1-0B	0.392	0.498	0.364	0.322	0.347–0.354
MgB-1-10B	0.425	0.422	0.393	0.340	0.367–0.384
MgB-1-20B	0.479	0.486	0.440	0.372	0.409–0.425

applied load is enough to create both elastic and plastic deformations [27]. Furthermore, it is seen from the table that the H_{HK} values of the samples are closer to the H_v values of the plateau (saturation) region. Therefore, Hays–Kendall model is the most appropriate model to determine the microhardness values and mechanical properties of the samples (Table 7).

3.4.5 IIC Model

The Indentation-Induced Cracking (*IIC*) model is developed to explain the *RISE* behavior in the samples [28]. In *RISE* behavior, hardness of the samples increases with applied loads. Although *RISE* has been observed in various samples, the reason still has not been fully explained. There are different approaches in the literature. It is expressed that during the loading, metallic samples can be hardened and cracking happens in fragile samples. According to Feltham and Banerjee, this behavior is related to the energy losses around the indenter [29]. The formation of cracks during indentation causes the release of the elastic deformation energy. This reduces the resistance of the sample to the indenter. Maximum depth of the applied test load is offset by the total sample resistance. This resistance can be expressed as

$$F = R_e + R_f + R_p + R_c \tag{13}$$

where F is the applied test load, R_e is the resistance due to elastic deformation, R_f is the resistance due to slip of the interface of the sample, R_p is the resistance due to plastic deformation, and R_c is the resistance due to cracks. The hardness value in this model can be expressed as

$$H_v = \lambda_1 K_1 \left(\frac{F}{d^2}\right) + K_2 \left(\frac{F^{5/3}}{d^3}\right) \tag{14}$$

Here, d is the diameter of the trace, and λ_1, K_1, and K_2 are constants. While K_2 is load-dependent, K_1 is a constant dependent on the indenter geometry. For ideal plastic materials, $\lambda_1 = 1$, $K_2 = 0$; but for perfect brittle solids $\lambda_1 = 0$. If the sample being tested is fragile, only the second portion of the equation is used. In this study, in all the samples (except *05-20B MgB*) elastic deformation is observed. It means that the fragility is high. In this model, the hardness values of the samples are calculated by using Eq. (15).

$$H_v = K \left(\frac{F^{5/3}}{d^3}\right)^m \tag{15}$$

where K and m values are independent of load and can be calculated using $\ln(H_v)$ versus $\ln(F^{5/3}/d^3)$ graph shown in Fig. 8. The constant m is indicative of the *ISE/RISE* behavior of the samples. For $m > 0.6$, the sample shows normal *ISE* behavior, but for $m < 0.6$, it obeys *RISE* behavior. Table 8 shows the calculated values of the parameters. It is seen that all the samples except *MgB-05-20B* obey *RISE* behavior, whereas it exhibits *ISE* behavior. Analyzing data in Table 8, it can be seen that *IIC* model

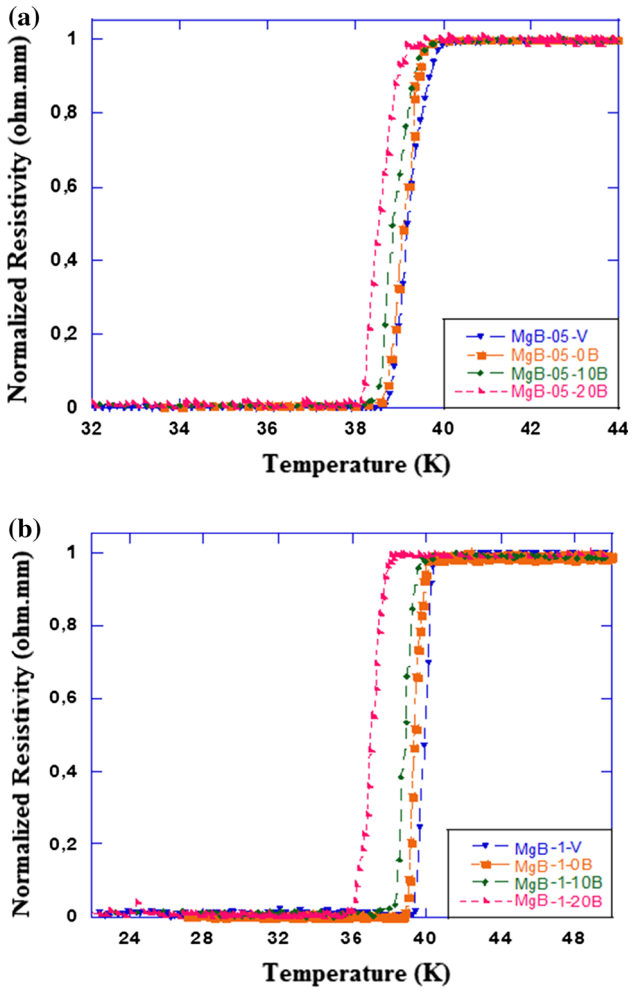

Fig. 9 Normalized resistivity curves as a function of temperature for the samples **a** for 0.5 h annealing time, **b** for 1 h of annealing time

hardness values are close to hardness values of the plateau region for samples exhibiting *RISE*. This result confirms that plastic deformation is dominant for the samples except *MgB-05-20B* which shows elastic deformation. The results of load-dependent Vickers microhardness at the plateau region and load-independent hardness values calculated using the *PSR*, *EPD*, *IIC* models and the *HK* approach are given in Table 9 in order to analyze them comparatively. As it can be seen from the table, *HK* approach is the most appropriate model for the *MgB-05-20B* sample that shows *ISE*, but *IIC* is the most appropriate model for all other samples that exhibit *RISE* behavior.

3.5 Resistivity measurements

The measurements of dc resistivity are performed with the four-probe method. Both voltage and current contacts are made with silver paint in order to minimize the contact resistance. We measured the temperature (10–50 K) dependence of resistivity of the samples running 5 mA dc current through the sample in the cryostat.

The temperature where the resistivity of the samples started to decrease sharply is determined to be the critical temperature (T_c^{onset}) of the samples obtained in this study. The transition temperature to superconductivity and the temperature where the resistivity drops to zero (T_c^{offset}) values are determined from ρ-T graphs (Fig. 9). As can be seen from the graph, the samples have metallic behavior above the T_c^{onset} transition temperature. The values of critical temperature vary partially as a function of the pressure.

In two series of MgB_2 samples, it is observed that the critical temperatures of the samples produced in vacuum are higher than those of the samples produced in Ar atmosphere. The values of T_c decrease with increasing applied pressure. T_c^{offset} is 40.00 and 39.99 K for *MgB-05-V* and *MgB-1-V* samples, respectively. These values decreased to values of 39.49 and 38.11 K for *MgB-05-20B* and *MgB-1-20B* samples, respectively. It can be said that the samples produced at 1 h annealing exhibit slightly lower T_c values compared to MgB-05 series. A reduction in T_c that occurs with pressure in superconducting metals is observed in several studies [30–33]. It is known that the pressure causes the decrease of T_c in BCS type simple metals. Up to the highest pressure value that is studied until now, the transition temperature decreased with pressure [34, 35]. The decrease of T_c with pressure support to the idea of BCS-type coupling originating from high phonon frequency of B element [36].

4 Conclusions

In this study, the structural, mechanical and superconducting properties of MgB_2 superconductors produced by the ex situ method are investigated. The samples are prepared in various atmospheres including vacuum, unpressurized Ar, 10 bar Ar, and 20 bar Ar with annealing times of 0.5 and 1 h. XRD and SEM analysis have been performed to determine the microstructural properties of the samples. Also microhardness measurements are performed to determine the mechanical properties of the samples. Meyer's law, *PSR*, *EPD*, *HK*, and *IIC* models are applied in order to determine the most suitable model to explain the mechanical properties of the samples.

- *a* and *c* parameters of MgB_2 superconductor produced have the highest values in *MgB-V* series. By introducing Ar and by increasing the applied Ar pressure, a significant decrease of the lattice parameters is observed. The lowest values of the lattice parameters are observed in *MgB-05* series. This result is consistent

with the results in the literature because it is known that pressure has shortening effect on the distances between the bonds.

- The grain sizes of the samples decrease with the presence of Ar and increasing pressure. Reduction in grain sizes can be related to the densification effect of pressure during grain growth. The samples produced in 0.5 h have smaller grains than the ones annealed for 1 h, consistent with previous studies. Increasing the annealing time cause larger grain formation due to thermal expansion during the process. Also, these results are confirmed by SEM images.
- The characteristic morphology of granular structure of MgB_2 is observed by SEM images. In this granular structure, the grain sizes are different from each other and agglomerations are observed in some places. Also there is a specific orientation of the particles in the sample.
- A decrease in the grain sizes (especially for *MgB-05-20B* and *MgB-1-20B*) causes reduction of voids between particles, so that one can obtain a stronger connection between grains. The decrease of porosity causes the samples to become mechanically harder. This result is confirmed by Vickers microhardness measurements.
- According to the Vickers microhardness measurements, it is seen that the microhardness values of the samples are load-dependent. Excluding *MgB-05-20B*, the hardness values of all the samples increased with increasing applied loads. This behavior is referred to as *RISE* in the literature. The hardness of the *MgB-05-20B* sample decreased with increasing load showing indentation size effect (*ISE*). Also the samples produced in 0.5 h were found to be harder than the samples produced in 1 h. This result may be related with increasing the voids in the samples due to increasing annealing time.
- In the series of 0.5 h, elastic modulus, yield strength and fracture toughness values of the samples produced in Ar atmosphere without pressure are higher than the values of the samples produced in vacuum. By the reaching the values of 10 and 20 bar, respectively, *E*, *Y*, and K_{IC} values increased. Also in *MgB-05-V*, *MgB-05-0B*, and *MgB-05-10B* samples; *E*, *Y*, and K_{IC} values increased with increasing applied load. However, in *MgB-05-20B* sample, these values decreased with the increasing the applied load. This result is associated with *ISE* behavior.
- *HK* is found to be most appropriate model for *MgB-05-20B* sample that obeys *ISE* behavior; *IIC* is found to most suitable model for the rest of the samples that show *RISE* behavior. So *MgB-05-20B* sample shows both plastic and elastic deformation; and all the other samples show only plastic deformation.
- The resistivity measurements reveal that the critical temperatures of the samples produced in vacuum are higher than those of the samples produced in Ar atmosphere. The values of T_c decrease with increasing applied pressure.

Acknowledgments This research has been supported by Kastamonu University Scientific Research Projects Coordination Department under the Grant No. KUBAP-03/2012-03.

References

1. K. Sangwal, Mater. Chem. Phys. **63**, 145 (2000)
2. J. Gong, H. Miao, Z. Zhao, Z. Guan, load-dependence of the measured hardness of Ti (C, N)-based cermets. Mater. Sci. Eng. A **303**, 179 (2001)
3. B. Basu, N. Mukhopadhyay, K. Manisha, J. Eur. Ceram. Soc. **29**, 801 (2009)
4. O. Şahin, O. Uzun, U. Kölemen, N. Uçar, J. Phys. Condens. Matter **19**, 306001 (2007)
5. K. Sangwall, B. Surowska, P. Blaziak, Mater. Chem. Phys. **77**, 511 (2002)
6. D.D. Graaf, M. Braciszewicz, H.T. Hintzen, M. Sopicka-Lizer, G. De With, J. Mater. Sci. **39**, 2145 (2004)
7. R.K. Marwaha, B.S. Shah, Cryst. Res. Technol. **23**, 63–65 (1988)
8. R. Bajpai, S.C. Datt, Indian J. Pure Appl. Phys. **24**, 254 (1986)
9. G. Constantinidis, R.D. Tomlinson, H. Neumann, Mag. Lett. **57**, 91 (1988)
10. C. Ascheron, C. Haase, G. Kuhn, H. Neumann, Cryst. Res. Technol. **24**, 33–35 (1989)
11. J. Schmidt, W. Schnelle, Y. Grin, R. Kniep, Solid State Sci. **5**, 535–539 (2003)
12. U. Kölemen, J. Alloys Compd. **425**, 429–435 (2006)
13. T. Prikhna, W. Gawalek, Y. Savchuk, N. Sergienko, V. Moshchil, S. Dub, V. Sverdun, L. Kovalev, V. Penkin, M. Zeisberger, M. Wendt, G. Fuchs, T. Habisreuther, D. Litzkendorf, P. Nagorny, V. Melnikov, Phys. C. **595**, 460–462 (2007)
14. M. Dogruer, O. Gorur, Y. Zalaoglu, O. Ozturk, G. Yildirim, A. Varilci, C. Terzioglu, J. Mater. Sci. Mater. Electron. **24**, 352–361 (2013)
15. L. Arda, O. Ozturk, E. Asikuzun, S. Ataoglu, Powder Technol. **235**, 479–484 (2013)
16. M. Tosun, S. Ataoglu, L. Arda, O. Ozturk, E. Asikuzun, D. Akcan, O. Cakiroglu, Mater. Sci. Eng. A **590**, 416–422 (2014)
17. E. Asikuzun, O. Ozturk, H.A. Cetinkara, G. Yildirim, A. Varilci, M. Yılmazlar, C. Terzioglu, J. Mater. Sci. Mater. Electron. **23**, 1001–1010 (2012)
18. B. Ozkurt, J. Supercond. Nov. Magn. **27**, 2407–2414 (2014)
19. H. Koralay, A. Arslan, S. Cavdar, O. Ozturk, E. Asikuzun, A. Gunen, A.T. Tasci, J. Mater. Sci. Mater. Electron. **24**, 4270–4278 (2013)
20. H. Aydın, A. Babanli, S.P. Altintas, E. Asikuzun, N. Soylu, O. Ozturk, M. Dogruer, C. Terzioglu, G. Yildirim, J. Mater. Sci. Mater. Electron. **24**, 4566–4573 (2013)
21. D. Tabor, J. Inst. Metals **79**, 1–18 (1951)
22. O. Sahin, O. Uzun, U. Kolemen, B. Duzgun, N. Ucar, Chin. Phys. Lett. **22**, 3137–3140 (2005)
23. J.B. Quinn, G.D. Quinn, J. Mater. Sci. **32**, 4331–4346 (1997)
24. M. L. Tarkanian, J.P. Neumann and L. Raymond, M. L. Tarkanian, J.P. Neumann, L. Raymond, in *The Science of Hardness Testing and Its Research Application*, ed. by J.H.

Westbrook and H. Conrad (American Society for Metals, Metal Park, OH, 1973), pp. 187–198
25. C. Hays, E.G. Kendall, Metallography **6**, 275–282 (1973)
26. N. Gane, F.P. Bowden, J. Appl. Phys. **39**, 1432–1435 (1968)
27. R. Awad, A.I. Abou-Aly, M. Kamal, M. Anas, J. Supercond. Nov. Magn. **24**, 1947–1956 (2011)
28. H. Li, R.C. Bradt, J. Mat. Sci. **31**, 1065–1070 (1996)
29. P. Feltham, R. Banerjee, J. Mat. Sci. **27**, 1626–1632 (1992)
30. D.U. Gubser, A.W. Webb, Phys. Rev. Lett. **35**, 104–107 (1975)
31. L.D. Jennings, C.A. Swenson, Phys. Rev. **112**, 31–43 (1958)
32. J. Wittig, Z. Phys. **195**, 27–215 (1966)
33. M.A. Il'ina, E.S. Itskevich, Zh. Eksp. Teor. Fiz. **61**, 2357–2361 (1971)
34. T. Vogt, G. Schneider, J.A. Hriljac, G. Yang, J.S. Abell, Phys. Rev. B **63**, 2205 (2001)
35. P. Bordet, M. Mezouar, M. Nunez-Regueiro, M. Monteverde, M.D. Nunez-Regueiro, N. Rogado, K.A. Regan, M.A. Hayward, T. He, S.M. Loureiro, R.J. Cava, Phys. Rev. B **64**, 2502 (2001)
36. J.E. Hirch, F. Marsiglio, Phys. Rev. B **64**, 144523 (2001)